Available online at www.sciencedirect.com
ScienceDirect
International Journal of Heat and Mass Transfer 50 (2007) 320–334
International Journal of HEAT and MASS TRANSFER
www.elsevier.com/locate/ijhmt

# Application issues of the streamline, heatline and massline for conjugate heat and mass transfer

Fu-Yun Zhao, Di Liu, Guang-Fa Tang *

*College of Civil Engineering, Hunan University, Changsha, Hunan 410082, PR China*

Received 10 January 2005; received in revised form 27 April 2006
Available online 1 September 2006

**Abstract**

Functions and lines have been extensively used to visualize two-dimensional fluid, heat and mass transportation structures. However, some ambiguities related to streamlines, heatlines and masslines still exist, especially for conjugate heat and mass transfer in anisotropic media. Present work aims to clarify these issues from numerical viewpoints, mainly including diffusion coefficient of transportation function at the interface of different media, different numerical approaches for solving visualization functions, non-dimensional forms of heatfunction and massfunction matching the spatial Nusselt and Sherwood numbers. The numerical procedures and code routines for the primitive conserved variables and the functions are illustrated through visualizing fluid, heat and solute transportations of double diffusive natural convection in square enclosures with massive walls or center-inserted body.


*Keywords:* Numerical visualization; Integration method; Poisson method; Conjugate heat and mass transfer

## 1. Introduction

Streamfunctions and streamlines are routinely the best way to visualize the fluid flow. The heatfunctions and heatlines as analogous concept for the visualization of heat transport were first introduced by Kimura and Bejan [1] and Bejan [2], and its mass counterpart, the massfunctions and masslines concept, by Trevisan and Bejan [3]. The streamline, heatline and massline are used for long time for visualization and analysis of fluid flow occurring in a two-dimensional moving medium, defining well-bordered corridors (fluid, energy and mass tubes respectively) where fluid, energy and mass flow. Heatline and massline have been used extensively to understand heat and mass transfer in various geometries and applicable ranges. Several great improvements are reviewed here.

Littlefield and Desai [4] extended heatfunction and heatline to cylindrical coordinates and illustrated laminar natural convection in a vertical annular space by similarity solutions. Bello-Ochende [5] constructed Poisson-type heatfunction equation analogous to the one used in computing the streamfunction, and investigated the response of the net energy trajectories to changes in the Rayleigh number as its value increases from the subcritical, through the threshold, to the postcritical values for the Benard-type configuration in a square cavity. Aggarwal and Manhapra [6,7] used heatlines for the numerical visualization of transient heat transfer in cylindrical enclosures. They computed non-dimensional heatfunction at any time integrating the first order derivatives of heatfunction. Not only can the heatlines provide a convenient instantaneous visualization of the heat flow, the value of the Nusselt number is also given. Ho and Lin [8] presented heatlines for steady laminar two-dimensional natural convection in concentric and eccentric horizontal cylindrical annuli with mixed boundary conditions. Afterwards, Ho and Lin [9] examined steady laminar natural convection of cold water in a vertical annulus with a constant-heat-flux heated inner wall and an isothermally cooled outer wall, vividly

* Corresponding author. Tel.: +86 731 882 2760; fax: +86 731 882 2667.
*E-mail address:* zfycfdnet@163.com (G.-F. Tang).

0017-9310/$ - see front matter © 2006 Elsevier Ltd. All rights reserved.
doi:10.1016/j.ijheatmasstransfer.2006.06.026

**Nomenclature**

| | |
|---|---|
| $A$ | coefficient in difference equation |
| $C$ | concentration (kg/m$^3$) |
| $C$ | dimensionless concentration |
| $C_P$ | isobaric specific heat J/(kg K) |
| $D$ | mass diffusivity (m$^2$/s) |
| $f$ | geometric interpolation factor |
| $g$ | gravitational acceleration (m/s$^2$) |
| $i$, $j$ | nodal index along $x$ and $y$ axes, respectively |
| $J$ | transport flux |
| $k$ | thermal conductivity (W/m K) |
| $L$ | length of square enclosure (m) |
| $Le$ | Lewis number |
| $N$ | buoyancy ratio |
| NI, NJ | maximum nodal index along $x$ and $y$ axes |
| $Nu$ | overall Nusselt number |
| $p$ | pressure (N/m$^2$) |
| $P$ | dimensionless pressure |
| $Pr$ | Prandtl number |
| $Ra_t$ | thermal Rayleigh number |
| $R_D$ | solute diffusion coefficient ratio |
| $R_k$ | thermal conductivity ratio |
| $S$ | source term |
| $Sh$ | overall Sherwood number |
| $t$ | temperature (K) |
| $T$ | dimensionless temperature |
| $u$, $v$ | velocity components in $x$, $y$ directions (m/s) |
| $U$, $V$ | dimensionless velocity components in $X$, $Y$ |
| $V_r$ | reference velocity scale |
| $x$, $y$ | Cartesian coordinates (m) |
| $X$, $Y$ | dimensionless Cartesian coordinates |

*Greek symbols*

| | |
|---|---|
| $\alpha$ | thermal diffusivity (m$^2$/s) |
| $\beta$ | volumetric expansion coefficient |
| $\Gamma$ | generic diffusion coefficient |
| $\Delta$ | difference value |
| $\mu$ | dynamic viscosity (kg/m s) |
| $\nu$ | kinematic viscosity (m$^2$/s) |
| $\rho$ | density (kg/m$^3$) |
| $\phi$ | generic intensive variable |
| $\Phi$ | generic function for visualization |
| $\Psi$ | streamfunction |
| $\xi$ | heatfunction |
| $\eta$ | massfunction |

*Subscripts*

| | |
|---|---|
| $e$ $w$ $n$ $s$ | four interfaces of control volume around $P$ |
| $E$ $W$ $N$ $S$ | four nodes adjacent to $P$ shown in Fig. 1 |
| F | values of the fluid domain |
| high (low) | higher (lower) value |
| $i$ | step function for fluid/solid regions |
| max, min | maximum, minimum |
| 0 | reference value or location |
| $P$ | at nodal point $P$ |
| $S$ | values of the solid domain |
| $x$, $y$ | referring Cartesian co-ordinates |
| $\phi$ | referring generic intensive variable $\phi$ |
| $\Phi$ | referring generic function $\Phi$ |

*Superscript*

| | |
|---|---|
| * | dimensionless |

visualizing by means of contour maps of heatlines and streamlines.

Morega and Bejan [10,11] used similarity variables to derive closed form expressions for heatlines in forced-convective boundary layers over flat plates in fluid media and fluid-saturated porous media, respectively. Costa [12] followed a similar approach to develop exact expressions for natural convection from vertical plates in the presence of both isothermal and isoflux boundary conditions.

Dash [13] developed the heatline concept for turbulent flows using the turbulent flux components, while Bejan [14, p. 361] did it adopting an effective diffusion coefficient that includes the eddy diffusivity for heat transfer when dealing with turbulent boundary layer flows.

Functions and lines used for visualization purposes can be unified from physical and numerical viewpoints, Costa [15] advocated a uniform formulation for the streamfunction, heatfunction and massfunction that is suitable for direct incorporation into a computational fluid dynamics code, including conjugate heat and mass transfer problems. Conjugate heat transfer problem comprising the tube wall as well as the gas stream was analyzed by Kim and Jang [16]. The harmonic mean conductivities at the interface between the tube wall and gas stream and at the interface between the tube wall and the insulation material were conducted respectively. Deng and Tang [17] defined functions in terms of dimensionless governing equations and modified the formulation at the solid–fluid boundaries in the work of Costa [15], considering that the diffusion coefficients of the function equations are invariant. However, some inconsistency was reported subsequently by Costa [18], confirming the accuracy of Costa's formulation of heatlines and masslines at the solid–fluid boundaries [15]. Costa [19] evolved the work of Costa [15] into the unification of the streamline, heatline and massline methods for anisotropic media. The numerical procedures and code routines designed for isotropic media need only slight modifications to deal with anisotropic media through fully implicit consideration due to the additional diffusive terms for transport phenomena in anisotropic media. Mukhopadhyay et al. [20] made the extension to the use of the heatlines and masslines in reacting flows, the conserved scalar variables being the total enthalpy (sum of sensible enthalpy and enthalpy of reaction) and atomic mass

fractions of the individual elements. Mukhopadhyay et al. [21] unified the formulations for heatline and massline calculations in terms of conserved scalars, such as enthalpy and elemental mass fractions in reacting and non-reacting jets. Their work has also been included in the unified visualization methods for anisotropic media [19].

Except these improvements made to enlarge the applicability of the heatlines and masslines, some other important investigations have been conducted, including spherical configuration [22], discrete heat sources [23], heat and mass diffusive walls [24] and parallelogrammic enclosures [25,26].

However, in spite of its broader applications, some of the implementational issues related to streamlines, heatlines and masslines are not clarified, including different numerical solution strategies for visualization function lines, diffusion coefficient of transportation function at the interface of different media, values of streamfunction, heatfunction and massfunction in isolated solid block, non-dimensional forms of heatfunction and massfunction respectively matching the spatial heat and mass transferring parameters. The main objective of this work is to present treatments for these issues. For the sake of simplicity, the solution strategies and routine codes are illustrated by two-dimensional laminar double diffusive natural convection in square enclosures with massive walls or an inserted body. However, without loss of generality, the method and results could be straightforwardly extended to porous media, turbulent flows, reacting flows and complex geometries.

## 2. Unification of streamfunction, heatfunction and massfunction

Two-dimensional fluid flow, heat and mass transfer are usually described by partial differential equations, which can be written in the general conservative form [27, p. 16]

$$\frac{\partial \rho u \phi}{\partial x} + \frac{\partial \rho v \phi}{\partial y} = \frac{\partial}{\partial x}\left(\Gamma_\phi \frac{\partial \phi}{\partial x}\right) + \frac{\partial}{\partial y}\left(\Gamma_\phi \frac{\partial \phi}{\partial y}\right) + S_\phi \tag{1}$$

Variable $\phi$ is the specific transported variable, and some particular meanings of $\phi$ can be found in references [13–15,17,19,20,27]. They are also presented in Table 1. The recognition that all the relevant differential equations for fluid flow, heat and mass transfer, turbulence and related phenomena can be thought of as particular cases of the general $\phi$ equation is an important time-saving step. Mostly, we only need to concern about the numerical solution of Eq. (1).

Table 1
Diffusion coefficients and source terms for general variable $\phi$ in Eq. (1) for conjugate heat and mass transfer

| Physical principle | $\phi$ | $\Gamma_\phi$ | $S_\phi$ |
|---|---|---|---|
| Continuity | 1 | 1 | 0 |
| $x$ momentum equation | $u$ | $\mu$ | $-\frac{\partial p}{\partial x}$ |
| $y$ momentum equation | $v$ | $\mu$ | $-\frac{\partial p}{\partial y} + \rho g \beta_t (t - t_0) + \rho g \beta_c (c - c_0)$ |
| Energy conservation (fluid side) | $t_F$ | $k_F/C_{PF}$ | 0 |
| Energy conservation (solid side) | $t_S$ | $k_S/C_{PF}$ | 0 |
| Species conservation (fluid side) | $c_F$ | $(\rho D)_F$ | 0 |
| Species conservation (solid side) | $c_S$ | $(\rho D)_S$ | 0 |

### 2.1. Conjugate heat and mass transfer

If the fluid flow subsides (stagnant fluid or solid medium with $u = v = 0$), the corresponding diffusion situation is described by the right hand side of Eq. (1), such as $k/C_P$ and $\rho D$ stand for the heat and species mass diffusion coefficients over the involved medium. When conjugate heat and mass transfer problems are solved using the SIMPLE-like algorithms in a unitary computational domain containing both the solid and fluid regions, one should pay attention to ensure the continuity of heat and mass fluxes at the solid–fluid interface.

In order to clarify this point, a simple conjugate heat transfer problem, i.e., the steady two-dimensional convection–conduction heat transfer across a planar interface separating the solid and fluid regions, is studied. The following form of energy equation without source term is employed to conform the general Eq. (1):

$$\frac{\partial \rho u t}{\partial x} + \frac{\partial \rho v t}{\partial y} = \frac{\partial}{\partial x}\left(\frac{k}{C_P}\frac{\partial t}{\partial x}\right) + \frac{\partial}{\partial y}\left(\frac{k}{C_P}\frac{\partial t}{\partial y}\right) \tag{2}$$

As expected, Eq. (2) is applicable to both the fluid and solid regions. However, when the conjugate heat transfer problem is solved numerically using Eq. (2) in the unitary computational domain, one has to pay close attention to ensure the continuity of heat flux at the solid–fluid interface. As noted by Patankar [27, p. 44] the harmonic mean of $(k/C_P)_F$ and $(k/C_P)_S$ and the piecewise-linear temperature profile have been adopted to evaluate the diffusion flux at the interface in order to ensure the overall balance of the computed results. Consequently, both solid and fluid specific heats ($C_{PS}$ and $C_{PF}$) would affect the diffusion flux at the interface and the computed temperature field. However, heat conduction only occurs in the solid region, the actual temperature field should be independent of the solid specific heat. Hence, the computed temperature field based on both solid and fluid specific heats will be physically incorrect for the case of $C_{PS} \neq C_{PF}$, although many authors have ignored this slight problem when treating with conjugate heat transfer problems [15–17,23,28]. If great difference in the values of the solid and fluid specific heats is involved in the computation, appreciable discontinuity of the heat flux will appear at the solid–fluid interface and serious error will be introduced in the computational results [28]. A simple but very efficient approach to avoid this error is that: the thermal conductivity $k$ in Eq. (2) is taken to be its actual value in the solid or fluid region, but the specific heat of the solid region $C_{PS}$ is artificially set to be equal to that of the fluid region $C_{PF}$ [29,30, p. 486]. As a result, the actual solid specific heat $C_{PS}$ will not affect

the computed temperature field, i.e., the diffusion flux at the interface would depend on $k_F/C_{PF}$ and $k_S/C_{PF}$, and the heat flux continuity can be ensured at the fluid–solid interface. The reason for choosing the specific heat of fluid ($C_{PF}$) instead of that of solid ($C_{PS}$) is that the specific heat affects the results only through the convection term of the energy equation (2), thus only the fluid specific heat is important.

The mass transfer problem consists of solving the following Eq. (3) for the concentration field and determining the mass fluxes associated with the concentration field from the Fick's law [14, p. 473].

$$\frac{\partial \rho uc}{\partial x}+\frac{\partial \rho vc}{\partial y}=\frac{\partial}{\partial x}\left(\rho D\frac{\partial c}{\partial x}\right)+\frac{\partial}{\partial y}\left(\rho D\frac{\partial c}{\partial y}\right) \tag{3}$$

From the outset, it is worth noting the similarities between the mass convection problem and the thermal convection problem. The latter consists of determining the temperature field from the energy equation (2) and the heat fluxes from Fourier's law of thermal diffusion. Eqs. (2) and (3) show that the concentration $c$ occupies the place of temperature, while the mass diffusivity $D$ replaces the thermal diffusivity $\alpha(k/\rho C_P)$, instead of $k/C_P$. Thus, the aforementioned specific heat problem in conjugate heat transfer would not be encountered in conjugate mass transfer.

If fluid flows involving anisotropic medium, such as porous medium, chemical species transportation, unified formulation for conjugate heat and mass transfer can be found in Costa [19] and Mukhopadhyay et al. [20,21] respectively.

### 2.2. Streamfunction, heatfunction and massfunction

The general unification procedure for the streamfunction, heatfunction and massfunction applies only to differential equations without source terms [15]. If the differential equation for a given variable presents a non-zero source term, conserved variables (such as total enthalpy and elemental mass fractions) should be used to express the scalar transport in terms of homogenous differential equations [20,21]. Present work only focuses on the issues related to the differential energy and mass equations without source terms. By invoking the differential mass conservation equation, Eq. (1) without source term can be written as

$$\frac{\partial}{\partial x}\left[\rho u(\phi-\phi_0)-\Gamma_\phi\frac{\partial \phi}{\partial x}\right]+\frac{\partial}{\partial y}\left[\rho v(\phi-\phi_0)-\Gamma_\phi\frac{\partial \phi}{\partial y}\right]=0 \tag{4}$$

the $\phi_0$ is introduced by the fact that any variable other than the pressure or the velocity components is made dimensionless as $(\phi-\phi_0)/\Delta\phi$, $\Delta\phi$ being the variable scale in the domain [14,31]. As noted by Trevisan and Bejan [3], the heatline and massline would exhibit the "centrosymmetry property" of streamline and isotherm/concentration patterns of convection in enclosures with centrosymmetric boundary conditions if the reference values $\phi_0$ ($t_0$ and $c_0$) were enclosure averaged quantities. In addition, the heatline and massline patterns would not be unique, because a new pattern can be plotted for each new reference temperature/concentration that are used to specify $t$ and $c$ numerically.

Defining the function $\Phi(x,y)$ through its first order derivatives as

$$\frac{\partial \Phi}{\partial y}=J_{\phi,x}=\rho u(\phi-\phi_0)-\Gamma_\phi\frac{\partial \phi}{\partial x} \tag{5a}$$

$$-\frac{\partial \Phi}{\partial x}=J_{\phi,y}=\rho v(\phi-\phi_0)-\Gamma_\phi\frac{\partial \phi}{\partial y} \tag{5b}$$

the new function $\Phi(x,y)$ is such that a constant $\Phi$ line is parallel to the flux flow $J_\phi$, or the flux across the constant line is zero, which can be expressed as

$$\mathrm{d}\Phi=J_\phi\times \mathrm{d}s=-J_{\phi,y}\,\mathrm{d}x+J_{\phi,x}\,\mathrm{d}y \tag{6}$$

Elementary segment d$s$ is crossed by the flux flow $J_\phi$. If d$\Phi$ equals 0, it means that there is not any $\phi$ flow crossing segment d$s$. In other words, constant $\Phi$ line is a non-crossed line by the $\phi$ flow, being thus a line that is tangent to the flow vector. Some characteristics of function $\Phi$ lines can be summarized as follows [15,17,19],

- A difference $\Delta\Phi$ between the $\Phi$ lines at two points represents the $\phi$ flow that crosses the segment linking these points by unit depth, being thus specially instructive the streets comprised between two constant $\Phi$ lines, in which well bordered $\phi$ flows are transferred.
- The $\Phi$ function is defined through its first order derivatives, Eqs. (5a) and (5b), being thus only important differences on the $\Phi$ values but not the $\Phi$ level. This relative behavior is similar to that of pressure when evaluating incompressible fluid flows, with a total freedom to choose any suitable reference point.
- As the $\phi$ flow flux cannot approach infinity, the area between the $\Phi$ lines cannot be zero, and then a constant $\Phi$ line either starts and ends on boundaries or circulates into vortices.
- The function $\Phi(x,y)$ can represent the strength of transportation, thus being relativities of convection ($\rho u(\phi-\phi_0)$, $\rho v(\phi-\phi_0)$) and diffusion ($-\Gamma_\phi\frac{\partial\phi}{\partial x}$, $-\Gamma_\phi\frac{\partial\phi}{\partial y}$). For example, heatfunction can determine which mode dominates the heat transportation, heat convection or heat conduction [1–26].

Assuming now that $\phi$ is a continuous function to its second order derivatives, the equality of its second order cross derivatives can be established through the expressions obtained from the right hand sides presented in Eqs. (5a) and (5b), leading to Eq. (7),

$$\frac{\partial}{\partial x}\left(\frac{1}{\Gamma_\phi}\frac{\partial \Phi}{\partial x}\right)+\frac{\partial}{\partial y}\left(\frac{1}{\Gamma_\phi}\frac{\partial \Phi}{\partial y}\right)+\frac{\partial}{\partial x}\left(\frac{\rho v}{\Gamma_\phi}(\phi-\phi_0)\right)-\frac{\partial}{\partial y}\left(\frac{\rho u}{\Gamma_\phi}(\phi-\phi_0)\right)=0 \tag{7}$$

This is the second order partial differential equation from which it will be evaluated the $\Phi$ field, for any particular corresponding meaning of variable $\phi$ [15]. It is an equation corresponding to a conduction-type problem, with source term if the fluid flow subsists and without source term if the fluid flow subsides, with the diffusion coefficient $\Gamma_\Phi$, where

$$\Gamma_\Phi = 1/\Gamma_\phi \tag{8}$$

As noted by Costa [15], the function diffusion coefficient $\Gamma_\Phi$ is maintained within parenthesis in Eq. (7) because it is a variable and not a constant in general case. One can obtain the streamfunction if $\phi_0 = 0$, $\phi = 1$ and $\Gamma_\phi = 1$ as shown in Table 1. However, preceding authors assume $\Gamma_\phi$ as 0 [17,21], thus it would lead to error, being that denominator would not be zero. Costa [15] has treated $\Gamma_\phi$ as a small constant number, which is similar as this. But the small constant number would lead to float errors during calculations.

Eq. (7) is a conduction-type equation. Solution for each particular $\Phi$ can be obtained following the same procedures as for variable $\phi$, once the boundary conditions for $\Phi$ are established. A unified treatment for the functions used for visualization purposes is now finished from a physical viewpoint [15]. The particular meaning of $\Phi$ for some usual cases are including streamfunction $\Psi$, heatfunction $\xi$ and species massfunction $\eta$. The coupling of general variable $\phi$ and function $\Phi$ has also been conducted by Bejan [14, p. 22, p. 505], Costa [15], Deng and Tang [17], Costa [19] and Mukhopadhyay et al. [20].

## 3. Numerical solution of flow field and $\phi$ fields

Excluding analytical and similarity solutions [4,10–12], there are primarily two methods to solve the incompressible fluid flow: vorticity-based method and primitive variables (pressure–velocity correction) method. For the former method, the velocity should be obtained from the known distributions of streamfunction or vorticity [8,9]. The velocity and vorticity were also solved integrally [1,3]. Bello-Ochende constructed a heatfunction that can be evaluated from vorticity and streamfunction [5]. There are, however, some major disadvantages to the streamfunction/vorticity method. The value of vorticity at a wall is difficult to specify and is often the cause of trouble in getting a converged solution. The pressure, which has been so cleverly eliminated, frequently happens to be an important desired result or even an intermediate outcome required for the calculation of fluid properties and momentum function. Therefore, the latter method, pressure–velocity correction, is applied broader [6,7,15–19,23–26] and adopted in the present study.

Typical control volumes employed for fluid flow variables are shown in Fig. 1, the velocity components are calculated for the points that lie on the faces of the control volume ($e$, $w$, $n$ and $s$), while the scalar variables and diffusion coefficients lie on the nodes, such as $P(i,j)$, $E(i+1,j)$, $W(i-1,j)$, $N(i,j+1)$ and $S(i,j-1)$, thus being a staggered

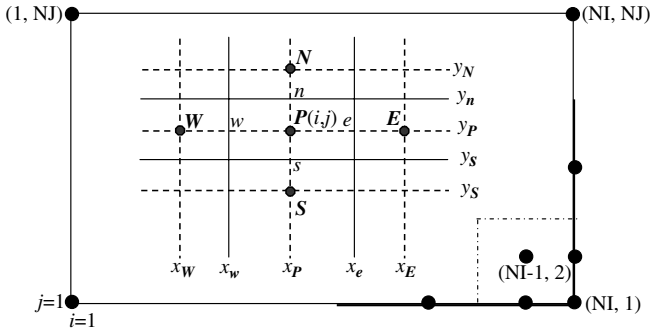


Fig. 1. Stencil of two-dimensional unit control volume (five-points discretization scheme) and type of FV grids on the boundary intersections.

grid system. So far, the specific information should be provided as to where the control volume faces are to be located in relation to the grid points. The usual practice is to define control volumes by a suitable grid and assign the computational node to the control volume center. However, for an alternative practice, one could as well (for structured grids) define the nodal locations first and construct control volumes around them, so that control volume faces lie midway between neighboring nodes. The advantage of the former practice is that the nodal value represents the mean over the control volume to higher accuracy (second order) than in the latter practice, since the node is located at the centroid of the control volume [27, p. 70, 30, p. 29, 32]. Additionally, for the conjugate heat and mass transfer problems, the former practice can be such that the fluid–solid interface forms a control volume face for the neighboring grid points. Thus the former approach is used more often [17] and will be adopted in the present study.

Governing equation (1) is discretized using finite volume method (FVM) on the aforementioned staggered grid system [27,30,32]. The third-order deferred correction QUICK scheme [30, p. 165, 32, 33] and second-order central difference scheme are, respectively, implemented for the convection and diffusion terms. The resulting discretized equations are solved by a line-by-line procedure, combining the tri-diagonal matrix algorithm (TDMA) and the successive over-relaxation (SOR) iteration. General equation (1) can be numerically solved by SIMPLE algorithm detailed in Patankar [27].

To solve the conjugate heat and mass transfer problem, the abrupt changes of diffusion coefficients at the interface between the fluid and solid regions are handled by harmonic mean formulation [27, p. 46, 31]. Additionally, the existence of the isolated block in the flow field would complicate the solution procedure. As far as FVM is concerned, there are several ways to treat the region of solid bodies as subsiding fluid, such as, large coefficient practice [29, 30, p. 244, 31, 32], large source-term practice [27, p. 145, 30, p. 245, 32] and viscosity coefficient practice [17, 27, p. 149, 30, p. 487, 32]. In the present work, large coefficient practice is adopted, i.e., the fluid and body regions are solved simultaneously by introducing a block parameter, which distinguishes a body region from a fluid region,

into discretized momentum equations. Thus convection terms are automatically turned off in the body region, thermal and solutal balances at the fluid–solid interface are carefully set up to make sure that the matching conditions of the following relations are satisfied.

$$k_F\left.\frac{\partial t}{\partial n}\right|_F = k_S\left.\frac{\partial t}{\partial n}\right|_S, \quad (\rho D)_F\left.\frac{\partial c}{\partial n}\right|_F = (\rho D)_S\left.\frac{\partial c}{\partial n}\right|_S \tag{9}$$

Additionally, special care must be taken to the use of the variable $\phi$ at the boundary intersections or sharp corners. Due to FVM is adopted, variables at these singular points are not required and updated for computing the flow field inside the domain. Thus they should be updated via interpolation or extrapolation from neighbor nodes. For example, at the node (NI, 1) presented in Fig. 1,

$$\phi(\mathrm{NI},1) = \phi(\mathrm{NI}-1,1) + \phi(\mathrm{NI},2) - \phi(\mathrm{NI}-1,2) \tag{10}$$

Similarly, $\phi(1,\mathrm{NJ})$ can be handled by the following relation:

$$\phi(1,\mathrm{NJ}) = \phi(1,\mathrm{NJ}-1) + \phi(2,\mathrm{NJ}) - \phi(2,\mathrm{NJ}-1) \tag{11}$$

Variables on other corners can also be handled as Eqs. (10) and (11). After these variables $\phi$ at the inner and boundary nodes have been obtained, the function $\Phi$ can be calculated by the following methods.

## 4. Numerical solution of function $\Phi$ fields

### 4.1. Integration method and Poisson method

For the integration method, Eqs. (5a) and (5b) are adopted [6,7,16,20,21,24]. The values of each function ($\Psi$, $\xi$ or $\eta$) are arbitrarily set to constants at reference point $(x_r, y_r)$. Using the values of functions at $(x_r, y_r)$, the values $\Phi(x, y_r)$ for points along the horizontal axis $(x, y_r)$ are computed by integration of Eq. (5b). Subsequently, using the function values $\Phi(x, y_r)$ at the axial points $(x, y_r)$, the functions are evaluated at other points along the row $(x, y)$ by integration of Eq. (5a). In fact, the integration paths can be chosen freely. The values of each point would be invariant for different integration paths because $\Phi$ is a potential function. It can also be written as

$$\Phi(x,y) = \Phi(x_r,y_r) + \int_{(x_r,y_r)}^{(x,y)} -\left[\rho v(\phi-\phi_0) - \Gamma_\phi\frac{\partial\phi}{\partial y}\right]\mathrm{d}x + \left[\rho u(\phi-\phi_0) - \Gamma_\phi\frac{\partial\phi}{\partial x}\right]\mathrm{d}y \tag{12}$$

For the Poisson method, the function $\Phi$'s Poisson equation (7) is used to solve each transport function [1,17–19,25]. The values of $\Phi$ over the boundaries are obtained by integrating the adequate $\Phi$ derivative presented in Eqs. (5a) and (5b) through the boundaries. Consequently, the Poisson method would be performed on the basis of the integration method.

### 4.2. Implementation of integration method

The function $\Phi(i_0,j_0)$ is assumed known as the reference value on the reference point $(i_0,j_0)$. Then, on the horizontal axial ($j = j_0$), it can be written that

$$\Phi_P = \Phi_W - [\rho v(\phi-\phi_0)]_W(x_w - x_W) - [\rho v(\phi-\phi_0)]_P(x_P - x_w) + \left(\Gamma_\phi\frac{\partial\phi}{\partial y}\right)_W(x_w - x_W) + \left(\Gamma_\phi\frac{\partial\phi}{\partial y}\right)_P(x_P - x_w) \tag{13}$$

For brevity, the $P$ and $W$ in Eq. (13) denote nodes $(i,j_0)$ and $(i-1,j_0)$ respectively, interface $w$ is among them. The stepwise profiles linking the $(i,j_0)$ and $(i-1,j_0)$ are adopted for each variable $\phi$. The piecewise-linear profiles can also be assumed, while they show little difference if flow field does not abruptly change or the grid lines are denser [29,31,32]. The first-order derivatives $\frac{\partial\phi}{\partial y}$ on $W$ and $P$ nodes can be obtained by central difference scheme. For example,

$$\left(\Gamma_\phi\frac{\partial\phi}{\partial y}\right)_P = (\Gamma_\phi)_P\frac{\phi_n - \phi_s}{y_n - y_s} \tag{14a}$$

Due to in-convenient implementation of boundary conditions for higher order schemes, the linear interpolation between the two nearest nodes is recommended,

$$\phi_n = f_n\cdot\phi_P + (1-f_n)\cdot\phi_N \tag{14b}$$

$$f_n = (y_N - y_n)/(y_N - y_P) \tag{14c}$$

Here $N$ and $S$ represent $(i,j_0+1)$ and $(i,j_0-1)$ respectively. The interpolation factor $f_n$ is a ratio defined in terms of the distances shown in Fig. 1. The interface variable $\phi_s$ can be obtained similarly as the $\phi_n$. Continuing integration on the vertical axial ($i = i_0$), it can be written that

$$\Phi_N = \Phi_P + [\rho u(\phi-\phi_0)]_P(y_n - y_P) + [\rho u(\phi-\phi_0)]_N(y_N - y_n) - \left(\Gamma_\phi\frac{\partial\phi}{\partial x}\right)_P(y_n - y_P) - \left(\Gamma_\phi\frac{\partial\phi}{\partial x}\right)_N(y_N - y_n) \tag{15}$$

Here $N$ and $P$ represent $(i,j+1)$ and $(i,j)$ respectively. The stepwise profiles linking the $N$ and $P$ are also adopted. Additionally, the first-order derivative $\frac{\partial\phi}{\partial x}$ on node $P$ can be calculated as following relations:

$$\left(\Gamma_\phi\frac{\partial\phi}{\partial x}\right)_P = (\Gamma_\phi)_P\frac{\phi_e - \phi_w}{x_e - x_w} \tag{16a}$$

$$\phi_e = f_e\phi_P + (1-f_e)\phi_E \tag{16b}$$

$$f_e = (x_E - x_e)/(x_E - x_P) \tag{16c}$$

The first-order derivative $\frac{\partial\phi}{\partial x}$ on node $N$ and variable $\phi_w$ can be similarly calculated to the ones in Eqs. (16a)–(16c), respectively. If the node $(i,j)$ in Eq. (15) corresponds to node $(i,j_0)$ in Eq. (13), after cyclic calculations and summing, the values of potential function $\Phi$ ($1 \leqslant i \leqslant \mathrm{NI}$, $1 \leqslant j \leqslant \mathrm{NJ}$) can be obtained, then done the contour lines.

As the preceding illustrations, original flow field variables $\phi$ on sharp corners should be updated via interpolation or extrapolation from the nearest nodes as done in Eqs. (10) and (11), because they are important when calculating the function $\Phi$. However, the function $\Phi$ on

boundary sharp corners cannot be contaminated by the singularities as it can be directly calculated via Eqs. (13) and (15). Extending this procedure to all the domain boundaries, starting from any suitable reference point $(x_r, y_r)$, then we have boundary conditions of first kind for $\Phi$ over all the domain boundaries [15,17].

### 4.3. Implementation of poisson method

The function $\Phi$ values on the boundaries are assumed known by integration along the boundaries via Eqs. (13) and (15). Following that, the Poisson Eq. (7) is discretized using FVM on the grid system presented in Fig. 1, and written as

$$A_P\Phi_P = A_E\Phi_E + A_W\Phi_W + A_N\Phi_N + A_S\Phi_S + S_\Phi \tag{17a}$$

$$A_P = A_E + A_W + A_N + A_S \tag{17b}$$

$$A_E = \frac{y_n - y_s}{x_E - x_P}(\Gamma_\Phi)_e, \quad A_W = \frac{y_n - y_s}{x_P - x_W}(\Gamma_\Phi)_w$$
$$A_N = \frac{x_e - x_w}{y_N - y_P}(\Gamma_\Phi)_n, \quad A_S = \frac{x_e - x_w}{y_P - y_S}(\Gamma_\Phi)_s \tag{17c}$$

$$\begin{aligned} S_\Phi = {} & [\rho v(\phi - \phi_0)]_e \cdot (\Gamma_\Phi)_e \cdot (y_n - y_s) \\ & - [\rho v(\phi - \phi_0)]_w \cdot (\Gamma_\Phi)_w \cdot (y_n - y_s) \\ & - [\rho u(\phi - \phi_0)]_n \cdot (\Gamma_\Phi)_n \cdot (x_e - x_w) \\ & + [\rho u(\phi - \phi_0)]_s \cdot (\Gamma_\Phi)_s \cdot (x_e - x_w) \end{aligned} \tag{17d}$$

Because the variable $\phi$ and function diffusion coefficient $\Gamma_\Phi$ are assumed on the nodes, those at the interfaces $e$, $w$, $n$ and $s$ should be interpolated or extrapolated from neighbor nodes. For variable $\phi$, the linear interpolation similar as Eqs. (14b) and (16b) can be adopted. However, for function diffusion coefficient $\Gamma_\Phi$, especially for conjugate heat and mass transferring, different interpolation practices have been involved in some discussions for domains with portions of different transport properties [15,17,18]. Actually, the diffusion coefficient $\Gamma_\Phi$ for $\Phi$ can be treated through any suitable practice similar to that used for the variable diffusion coefficient $\Gamma_\phi$ [27, p. 47, 32]. Among these, the harmonic mean practice shows to be the most attractive one for the situations with sharp variations in the involved diffusion coefficients [15, 17, 27, p. 47, 29, 30, p. 82, 31, 32], ensuring continuity of function $\Phi$ and the flux flow $J_\phi$, as is the case of conjugated transport phenomena with a domain composed by contiguous and very different materials. Using the harmonic mean practice, the $\Gamma_\Phi$ at interfaces $e$ and $n$ can be written respectively as

$$(\Gamma_\Phi)_e = \left(\frac{1 - f_e}{(\Gamma_\Phi)_P} + \frac{f_e}{(\Gamma_\Phi)_E}\right)^{-1},$$
$$(\Gamma_\Phi)_n = \left(\frac{1 - f_n}{(\Gamma_\Phi)_P} + \frac{f_n}{(\Gamma_\Phi)_N}\right)^{-1} \tag{18}$$

Function diffusion coefficients at other interfaces can be done similarly as in Eq. (18). It should be noticed that, if the integration method were applied to the case of conjugate heat and mass transportations, values of function diffusive coefficient $\Gamma_\Phi$ (and the relevant harmonic mean practices) at the interfaces are not required in Eqs. (12), (13) and (15).

## 5. Other issues on the streamfunction, heatfunction and massfunction

### 5.1. Function values in the impermeable solid region

Conjugate heat and mass transfer problem involves multiply-connected regions, where streamfunction $\Psi$ may be multiple-valued. The most usual case, however, is that in which the multiple connectedness is caused by the insertion of an obstacle in the flow, since there is no net flow of fluid through the obstacle, $\oint d\Psi = 0$, so that in such a case $\Psi$ remains single-valued. In other words, if the fluid flow subsides in the impermeable solid, $\Psi$ would maintain constant.

However, the heatfunction and massfunction both are composed of convection and diffusion terms. Heat and mass flows can occur in both fluid and solid regions. As a result, values of heatfunction and massfunction in solid blocks would not maintain constants. Particularly, the heatlines and masslines would become identical to the heat-flux lines and mass-flux lines respectively, and employed frequently to the studies of conduction and diffusion phenomena [14, p. 23, 19].

### 5.2. Spatial evaluation of heat and mass transfer

If heatfunction and massfunction were properly made dimensionless according with the concrete problems, their dimensionless values would be closely matching the spatial generalizations of the Nusselt and Sherwood numbers, respectively. More recently, there have been many studies in which the Nusselt number and Sherwood number are defined (integrated) along a plane drawn through the convective fluid, for example, through the mid-plane of an enclosure with double diffusive natural convection [34,35]. In this new kind of Nusselt number, the heat transfer rate is calculated as a superposition of convection and conduction, in the same way as in the construction of heatfunction. In other words, the heatfunction is a spatial generalization of the Nusselt number concept, in the sense that it describes the magnitude and direction of the heat transfer rate through any surface that can be imagined inserted in the convective medium. Similarly, the spatial Sherwood number can be defined by the massfunction. As an illustration, for steady double diffusive convection in the isotropic medium, the total spatial Nusselt number and Sherwood number on the vertical plane ($X = X_0$) can be expressed as

$$Nu_{X=X_0} = \int_{Y_1}^{Y_2} \left(\frac{\rho V_r L}{k/C_P} UT - \frac{\partial T}{\partial X}\right) dY,$$
$$Sh_{X=X_0} = \int_{Y_1}^{Y_2} \left(\frac{\rho V_r L}{(\rho D)} UC - \frac{\partial C}{\partial X}\right) dY \tag{19}$$

where $V_r$ and $L$ are velocity and length scales respectively. As expected, on the surface of a solid wall, the overall spatial Nusselt number and Sherwood number would degenerate into to the classical overall Nusselt number $\int_{Y_1}^{Y_2} -\frac{\partial T}{\partial X}\mathrm{d}Y$ and overall Sherwood number $\int_{Y_1}^{Y_2} -\frac{\partial C}{\partial X}\mathrm{d}Y$ respectively. Which attributes to that the convection terms in Eq. (19) are close to zero [1,3–7,10–12,16,17,19,24,26,31]. Similarly, those on the horizontal plane ($Y = Y_0$) inserted in the isotropic domain can also be defined as

$$Nu_{Y=Y_0} = \int_{X_1}^{X_2} \left(\frac{\rho V_r L}{k/C_P} VT - \frac{\partial T}{\partial Y}\right)\mathrm{d}X,$$
$$Sh_{Y=Y_0} = \int_{X_1}^{X_2} \left(\frac{\rho V_r L}{(\rho D)} VC - \frac{\partial C}{\partial Y}\right)\mathrm{d}X \tag{20}$$

The use of these expressions (Eqs. (19) and (20)) enables us to obtain conservative heat and mass transfer rates within the enclosure [35]. They include diffused and transported quantities that are integrated over the vertical (horizontal) axis in order to calculate the overall heat or mass transfer rates along this axis.

## 6. Applications and discussions

Fig. 2 presents three square enclosures ($L \times L$) and the two-dimensional Cartesian coordinate systems. The external vertical wall surfaces are maintained at constant and uniform different levels of temperature and concentration, thus giving rise to a double-diffusive free convective fluid flow. The horizontal walls are assumed to have zero thermal and mass diffusivities. Inner cavities and channels in these three cases are filled with the same fluid and pollutant, which are assumed to completely mixed Newton–Fourier fluid with thermal conductivity $k_F$ and mass diffusivity $D_F$. The hatched zones presented in Fig. 2 are assumed to be of the same and isotropic solid material with thermal conductivity $k_S$ and mass diffusivity $D_S$.

The scales and dimensionless variables are introduced,

$$V_r = \alpha/L, \quad \Delta t = t_{high} - t_{low}, \quad \Delta c = c_{high} - c_{low} \tag{21}$$
$$(X, Y) = (x, y)/L, \quad (U, V) = (u, v)/V_r, \quad T = (t - t_0)/\Delta t,$$
$$C = (c - c_0)/\Delta c, \quad P = p/\rho V_r^2 \tag{22}$$

where $\Delta t$ and $\Delta c$ are scales for temperature and concentration respectively [31,32]. Exercising these scales, one can obtain the following non-dimensional set of partial differential equations corresponding to Eqs. (1)–(3) [24,25],

Continuity equation

$$\frac{\partial U}{\partial X} + \frac{\partial V}{\partial Y} = 0 \tag{23}$$

$X$-momentum equation

$$\frac{\partial UU}{\partial X} + \frac{\partial VU}{\partial Y} = Pr\left(\frac{\partial^2 U}{\partial X^2} + \frac{\partial^2 U}{\partial Y^2}\right) - \frac{\partial P}{\partial X} \tag{24}$$

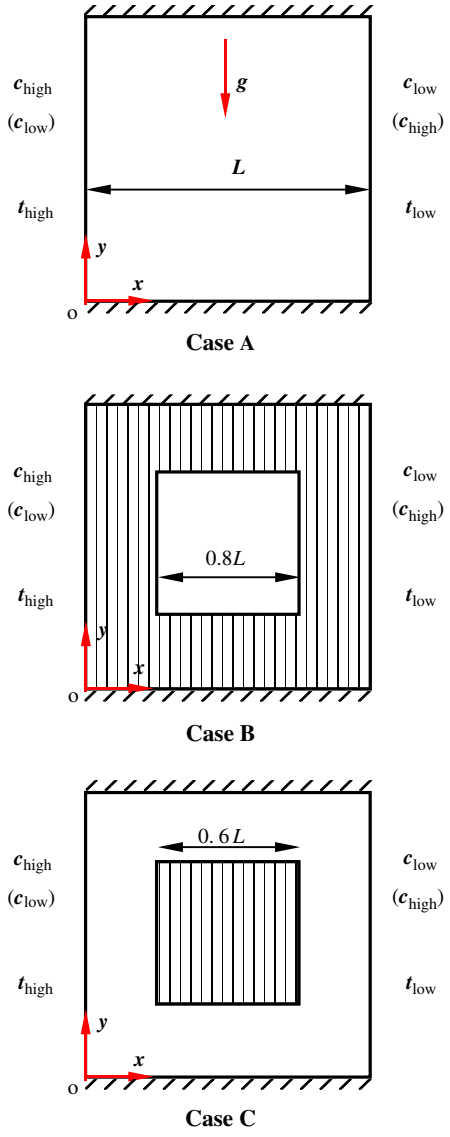


Fig. 2. Physical models and geometries for double diffusive conjugate heat and mass transfer.

$Y$-momentum equation

$$\frac{\partial UV}{\partial X} + \frac{\partial VV}{\partial Y} = Pr\left(\frac{\partial^2 V}{\partial X^2} + \frac{\partial^2 V}{\partial Y^2}\right) - \frac{\partial P}{\partial Y} + Ra_t Pr(T + NC) \tag{25}$$

Energy conservation equation on the fluid

$$\frac{\partial UT}{\partial X} + \frac{\partial VT}{\partial Y} = \left(\frac{\partial^2 T}{\partial X^2} + \frac{\partial^2 T}{\partial Y^2}\right) \tag{26}$$

Energy conservation equation on the solid blocks

$$0 = \frac{\partial^2 T}{\partial X^2} + \frac{\partial^2 T}{\partial Y^2} \tag{27}$$

Pollutant mass conservation equation on the fluid

$$\frac{\partial UC}{\partial X} + \frac{\partial VC}{\partial Y} = \frac{1}{Le}\left(\frac{\partial^2 C}{\partial X^2} + \frac{\partial^2 C}{\partial Y^2}\right) \tag{28}$$

Pollutant mass conservation equation on the solid blocks

$$0 = \frac{\partial^2 C}{\partial X^2} + \frac{\partial^2 C}{\partial Y^2} \tag{29}$$

The foregoing governing equations give rise to the dimensionless governing parameters,

$$Ra_t = g\beta_t L^3 \Delta t/\nu\alpha, \quad N = \beta_c \Delta c/\beta_t \Delta t,$$
$$Pr = \nu/\alpha, \quad Le = \alpha/D \tag{30}$$

where $N$ is the ratio between the solutal and thermal buoyancy forces. It can be either positive or negative, its sign depending on the ratio between the volumetric expansion coefficients $\beta_c$ and $\beta_t$. Assuming that $\beta_c > 0$ and $\beta_t > 0$, $N \geqslant 0$. Its limits are that it is null for no pollutant diffusion and infinite for no thermal diffusion. $N$ is assumed to be positive in the present work. Prescription of the temperatures and concentrations over the left and right walls can lead to a situation of combined or opposite global heat and mass flows. As illustrated in Fig. 2, if we impose the thermal condition that $t_{\text{left wall}}(T=1) > t_{\text{right wall}}(T=0)$, then for aiding flow $c_{\text{left wall}}(C=1) > c_{\text{right wall}}(C=0)$, and for opposing flow $c_{\text{left wall}}(C=0) < c_{\text{right wall}}(C=1)$.

For conjugate heat and mass transfer problem, thermal and solutal balances at the fluid–solid interfaces, Eq. (9), should be satisfied. Correspondingly, the heat and mass transfer diffusion coefficient ratios between the solid blocks and the medium that fills the enclosure should be introduced,

$$R_k = k_S/k_F, \quad R_D = (\rho D)_S/(\rho D)_F \tag{31}$$

Generally, for two-dimensional incompressible fluid and constant property situation, the first order derivatives of $\Phi$ in Eqs. (5a) and (5b) can be made dimensionless via the dimensionless function $\Phi^* = \Phi/\Gamma_\phi \Delta\phi$. Due to streamfunction $\Psi$ includes convection terms only, its dimensionless form can be written as

$$\Psi^* = \Psi/\rho V_r L \tag{32}$$

Thus, the dimensionless streamfunction equation can be obtained,

$$\frac{\partial \Psi^*}{\partial Y} = U, \quad -\frac{\partial \Psi^*}{\partial X} = V \tag{33}$$

The non-dimensional heatfunction $\xi$ and massfunction $\eta$ can be defined respectively as

$$\xi^* = \frac{\xi}{\Delta t\left(\frac{k}{C_P}\right)_F}, \quad \eta^* = \frac{\eta}{\Delta c(\rho D)_F} \tag{34}$$

Consequently, the dimensionless first order derivatives of heatfunction and massfunction equations can be obtained as follows:

On the fluid

$$\frac{\partial \xi^*}{\partial Y} = UT - \frac{\partial T}{\partial X}, \quad -\frac{\partial \xi^*}{\partial X} = VT - \frac{\partial T}{\partial Y} \tag{35}$$

$$\frac{\partial \eta^*}{\partial Y} = LeUC - \frac{\partial C}{\partial X}, \quad -\frac{\partial \eta^*}{\partial X} = LeVC - \frac{\partial C}{\partial Y} \tag{36}$$

On the solid blocks

$$\frac{\partial \xi^*}{\partial Y} = -R_k \frac{\partial T}{\partial X}, \quad -\frac{\partial \xi^*}{\partial X} = -R_k \frac{\partial T}{\partial Y} \tag{37}$$

$$\frac{\partial \eta^*}{\partial Y} = -R_D \frac{\partial C}{\partial X}, \quad -\frac{\partial \eta^*}{\partial X} = -R_D \frac{\partial C}{\partial Y} \tag{38}$$

As expected, after integrating along a vertical axis ($X = X_0$), their dimensionless values would be closely matching the spatial generalizations of the Nusselt and Sherwood numbers presented in Eq. (19) respectively [34–36]. If the Poisson method were adopted, the second-order partial differential equations corresponding to Eq. (7) across the anisotropic media (both fluid and solid blocks) can be written that

$$\frac{\partial^2 \Psi^*}{\partial X^2} + \frac{\partial^2 \Psi^*}{\partial Y^2} + \frac{\partial V}{\partial X} - \frac{\partial U}{\partial Y} = 0 \tag{39}$$

$$\frac{\partial}{\partial X}\left(\frac{1}{R_{ki}}\frac{\partial \xi^*}{\partial X}\right) + \frac{\partial}{\partial Y}\left(\frac{1}{R_{ki}}\frac{\partial \xi^*}{\partial Y}\right) + \frac{\partial}{\partial X}\left(\frac{VT}{R_{ki}}\right) - \frac{\partial}{\partial X}\left(\frac{UT}{R_{ki}}\right) = 0 \tag{40}$$

$$\frac{\partial}{\partial X}\left(\frac{1}{R_{Di}}\frac{\partial \eta^*}{\partial X}\right) + \frac{\partial}{\partial Y}\left(\frac{1}{R_{Di}}\frac{\partial \eta^*}{\partial Y}\right) + Le\left(\frac{\partial}{\partial X}\left(\frac{VC}{R_{Di}}\right) - \frac{\partial}{\partial X}\left(\frac{UC}{R_{Di}}\right)\right) = 0 \tag{41}$$

where $R_{ki}$ ($R_{Di}$) should be step-changed according with the different materials, i.e., $R_{ki} = R_{Di} = 1$ for fluid region, and $R_{ki} = R_k$ ($R_{Di} = R_D$) for solid blocks.

### 6.1. Code verification for double diffusive natural convection

The aforementioned numerical methods for solving variable $\phi(U, V, P, T \text{ and } C)$ and function $\Phi(\Psi^*, \xi^* \text{ and } \eta^*)$ are adopted. The convergence criterion is the maximal residual of all the governing equations is less than $10^{-5}$. In addition to the usual accuracy control, the accuracy of computations is also controlled using the energy and mass conservations within the system.

The computer code based on the mathematical model above is validated in three ways. The first considers double diffusive natural convection in a square cavity subjected from horizontal heat and mass fluxes [3]. A comparison of the results for $Ra_t = 3.5 \times 10^5$, $Pr = 0.7$ and 7.0, and $Le = 1$ may be found in Table 2, for this case the Nusselt

Table 2
Comparison of results for double diffusive natural convection in a two-dimensional cavity at $Le = 1$, $Ra_t = 3.5 \times 10^5$

| $N$ | $Pr$ | Trevisan and Bejan [3] | | Present study | |
|---|---|---|---|---|---|
| | | $Nu$ ($Sh$) | $Nu$ ($Sh$)$_{Y=0.5}$ | $Nu$ ($Sh$) | $Nu$ ($Sh$)$_{Y=0.5}$ |
| 0 | 7.0 | 4.83 | 5.88 | 4.86 | 5.81 |
| 0 | 0.7 | 4.78 | 5.82 | 4.82 | 5.75 |
| 1 | 7.0 | 5.73 | 6.83 | 5.75 | 6.79 |
| 1 | 0.7 | 5.72 | 6.87 | 5.73 | 6.75 |
| 3 | 7.0 | 6.88 | 8.05 | 6.84 | 7.88 |
| 3 | 0.7 | 6.76 | 7.92 | 6.75 | 7.96 |
| 9 | 7.0 | 8.67 | 9.86 | 8.50 | 9.58 |
| 9 | 0.7 | 8.44 | 9.55 | 8.40 | 9.43 |

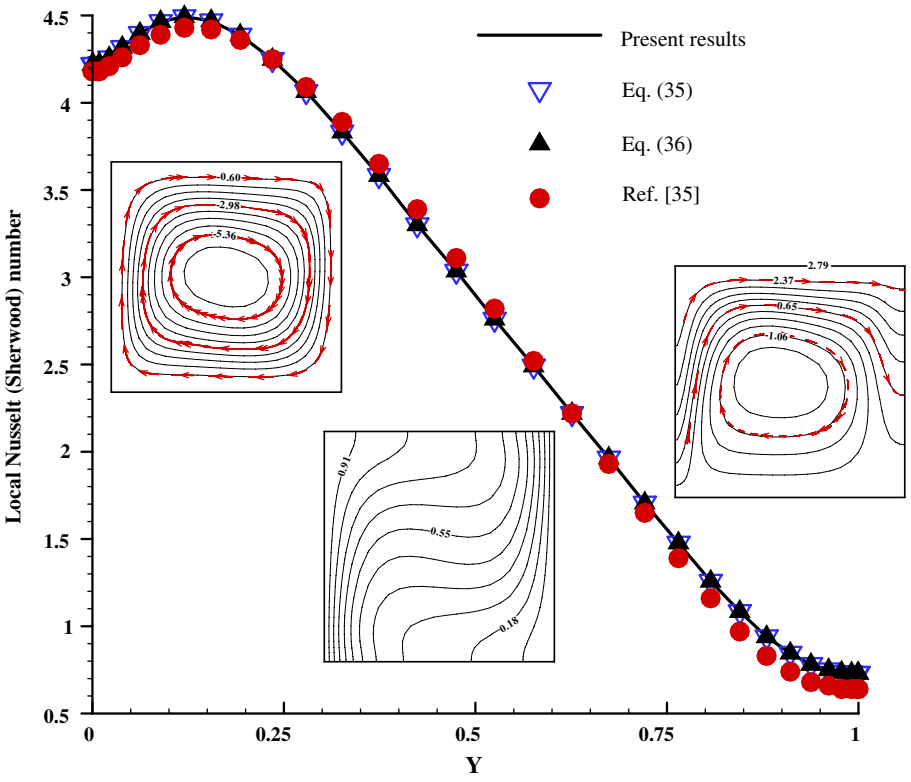


Fig. 3. Comparison for double diffusive convection in a square cavity ($Ra_t = 10^4$).

number and Sherwood number will be equivalent. The agreement between the present study and Trevisan and Bejan [3]'s results for $Le = 1$ is fairly good, with the largest Nusselt number difference around 4%. Second, the double diffusive convection in a square enclosure with constant temperature and concentration conditions is considered. The local Nusselt or Sherwood number distributions along the left vertical wall of the square cavity are compared with those of assisting flow with parameters of $Le = 1$, $Pr = 0.71$, $N = 1$ from Beghein et al. [35], shown in Fig. 3, together with the streamlines, isotherms (iso-concentrations) and heatlines (masslines). It is found that the excellent agreement has been achieved. Simultaneously, the gradients of heatfunction (massfunction) on the left wall match well with the local Nusselt (Sherwood) numbers, as demonstrated by Eqs. (35) and (36). The overall Nusselt number read as 2.79 from the heatline along the top wall approaches to 2.78 [35], which confirms Eq. (19). Additional comparisons ($N = 0$, $Ra_t = 10^4$–$10^6$, and $R_k = 10.0$) with the results of Kim and Viskanta [37] reveal agreement to within the accuracy with which their graphically presented Nusselt number data could be read.

Independence of solution on the grid size is studied for various cases, $Ra_t$, $N$, $Pr$, $Le$, $R_k$ and $R_D$. The grid is selected after some preliminary tests of asymptotic type. For instance, Table 3 shows the results for various thermal conductivity ratios and $Ra_t = 0$ and $10^5$ in case C illustrated in Fig. 2. In these calculations, the number of control volumes in each direction is varied from 6 to 22 in the body and 8 to 24 in each passageway between the body and the enclosure walls. The results show that grid independence is achieved above $40 \times 40$, showing acceptable differences in heat transfer rate (1%). In any case, $Nu$ ($Sh$) for various $R_k$ ($R_D$) shows similar trends as a function of grid size, ensuring the observed conclusion of grid independence. Grid refinement near the solid walls and bodies is used to accurately resolve large velocity, temperature and concentration gradients.

Table 3
Overall Nusselt (Sherwood) numbers for $N = 0$, $Le = 1.00$, $Pr = 0.71$ and different grids in case C

| (NI, NJ) | F–S–F | $Ra_t = 0$, $R_k = R_D$ | | | $Ra_t = 10^5$, $R_k = R_D$ | | |
|---|---|---|---|---|---|---|---|
| | | 0.2 | 1.0 | 5.0 | 0.2 | 1.0 | 5.0 |
| (24, 24) | 8–6–8 | 0.6034 | 1.0000 | 1.6411 | 4.6438 | 4.4739 | 4.1760 |
| (40, 40) | 14–10–14 | 0.6048 | 1.0000 | 1.6459 | 4.5856 | 4.4121 | 4.1096 |
| (52, 52) | 20–10–20 | 0.6049 | 1.0000 | 1.6461 | 4.5576 | 4.3856 | 4.0864 |
| (72, 72) | 24–22–24 | 0.6056 | 1.0000 | 1.6490 | 4.5536 | 4.3725 | 4.0623 |

### 6.2. Transportation structures and heat/mass transfer

The medium that fills the cavity is the moist air with a low concentration of water vapour, and one can take $Pr = 0.7$ and $Le = 0.8$. Subsequently, as $Le$ approaching unit, the local and global Sherwood numbers are always very close to the corresponding Nusselt numbers [25,35]. In following fluid, heat and mass transportation charts,

the intervals of streamlines, heatlines and masslines are $\Delta\Phi^* = (\Phi^*_{max} - \Phi^*_{min})/11$, where $\Phi$ stands for $\Psi$, $\xi$ or $\eta$.

*6.2.1. Case A – double diffusive natural convection in a square enclosure*

The streamlines, heatlines and masslines computed by Poisson method coincide with those from integration method completely, as illustrated in Fig. 4. The overall Nusselt and Sherwood numbers can be read directly from the heatlines and masslines along the top wall, such as $(Nu, Sh) = (1.33, 1.23)$, $(4.79, 4.30)$ and $(4.53, -4.07)$, respectively under $(Ra_t, N) = (10^3, 1.0)$, $(10^4, 10.0)$ with combined buoyancy effects and $(10^4, 10.0)$ with opposed buoyancy effects.

When thermal and solutal Rayleigh numbers are low ($10^3$), though they are combined, the heat and mass transfer through the enclosure occurs mainly by thermal conduction and solutal diffusion as shown in Fig. 4(a). Therefore, $Nu$ and $Sh$ equal 1.33 and 1.23 respectively, which corresponds to a conduction (diffusion) dominated regime because the Nusselt number and Sherwood number both have values of 1 for $Ra_t = 0$. The $\Psi^*_{min} = -2.07$ for the combined global heat and mass flows, is a little greater than that of pure thermal natural convection, $\Psi^*_{min} = -1.17$ presented by Deng and Tang [17], which indicates that convection is really weak. Therefore, the streamlines are of clockwise unicellular flow structure, heatlines and masslines both exhibit pseudo-conduction/diffusion structure as shown in Fig. 4(a). Besides this, the masslines crossing the higher-concentration wall are more crowded near the bottom side than those near the topside. This massline pattern visualizes the non-uniform distribution of the mass flux over the walls, which is different from the massline pattern provided by Trevisan and Bejan [3], in the case of uniform mass flux boundary conditions.

As combined heat and mass transfer strengthens greatly ($Ra_t = 10^4$, $N = 10$), streamlines presented in Fig. 4(b) have bicellular flow structure. It should be noted that, in terms

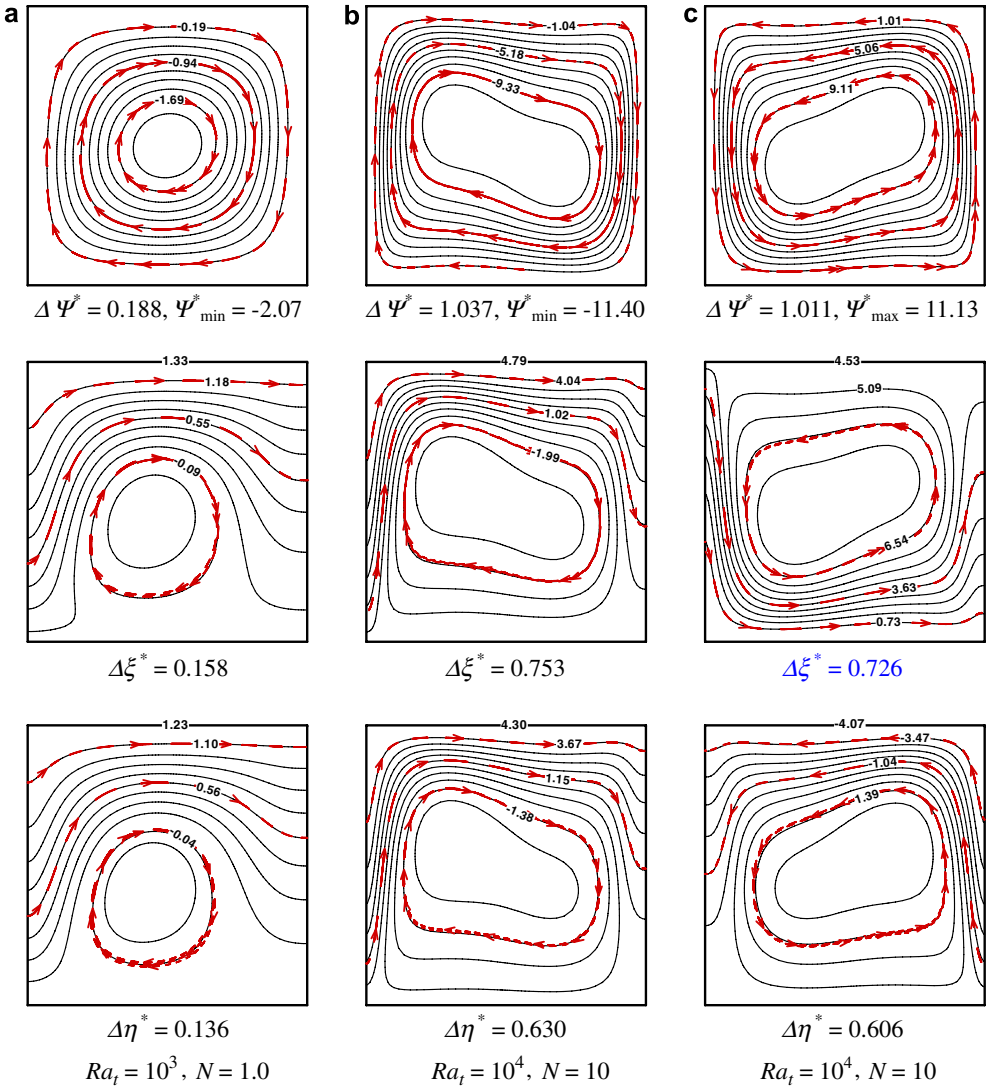


Fig. 4. Streamlines (top), heatlines (center) and masslines (bottom) for aiding (a and b) and opposing (c) buoyancy effects in Case A. Dashed and arrowed lines are computed by integration method, while solid lines are done by Poisson method.

of flow field, this nearly corresponds to a single natural convection heat transfer situation with $Ra_t = 10^5$. This is the expected behavior due to the $Ra_t Pr(T + NC)$ source term in the $Y$-momentum Eq. (25). $\Psi^*_{min} = -11.40$ for this situation approaches to $\Psi^*_{min} = -9.50$ for pure thermal natural convection in square cavity [17,28]. As expected, the overall Nusselt and Sherwood numbers both increase to higher values, 4.79 and 4.30 respectively. The non-uniform distribution of streamlines implies that the convection is strong in the boundary layer but weak in core where the fluid is almost stagnant. Convection has become a dominant mechanism to transport heat and mass, which is more clearly depicted by heatlines and masslines. The heatlines show a circulating core, with a global insulation effect over the cavity, the effective heat transfer occurring along a thin region near the top wall. Similarly, mass transport structures can be investigated by masslines.

Strong changes occur for the situation with opposite global heat and mass flows, as illustrated by Fig. 4(c). In what concerns flow structure, it comprises a major counter-clockwise vortex. As the main contribution is from the solutal buoyancy, and the highest concentration is at the right vertical wall, the thermosolutal convection induced flow takes place through counter-clockwise vortexes. The temperature and concentration contour plots (not shown) take the form of the mirror images corresponding to those associated with the pure natural convection heat transfer problem for $Ra_t = 10^5$, as well as the global Nusselt number, 4.53 in present situation and 4.52 in pure thermal natural convection [17,24]. The global Nusselt and Sherwood numbers are similar to those corresponding to the situations of combined buoyancy effects with $N = 10$. A drastic change occurs over the heatlines and masslines, presenting an anti-clockwise rotation. Heat flows now in the $X$ direction through the region close to the bottom wall. The closed counter-clockwise loop on the heatlines is placed near the left vertical wall, of highest temperature level. This is a direct consequence of the main flow occurring in the form of counter-clockwise vortexes. The solute flowing in the $X$ direction proceeds now from the right to the left, and flows over the narrow region close to the upper wall, as clearly shown by the masslines. The

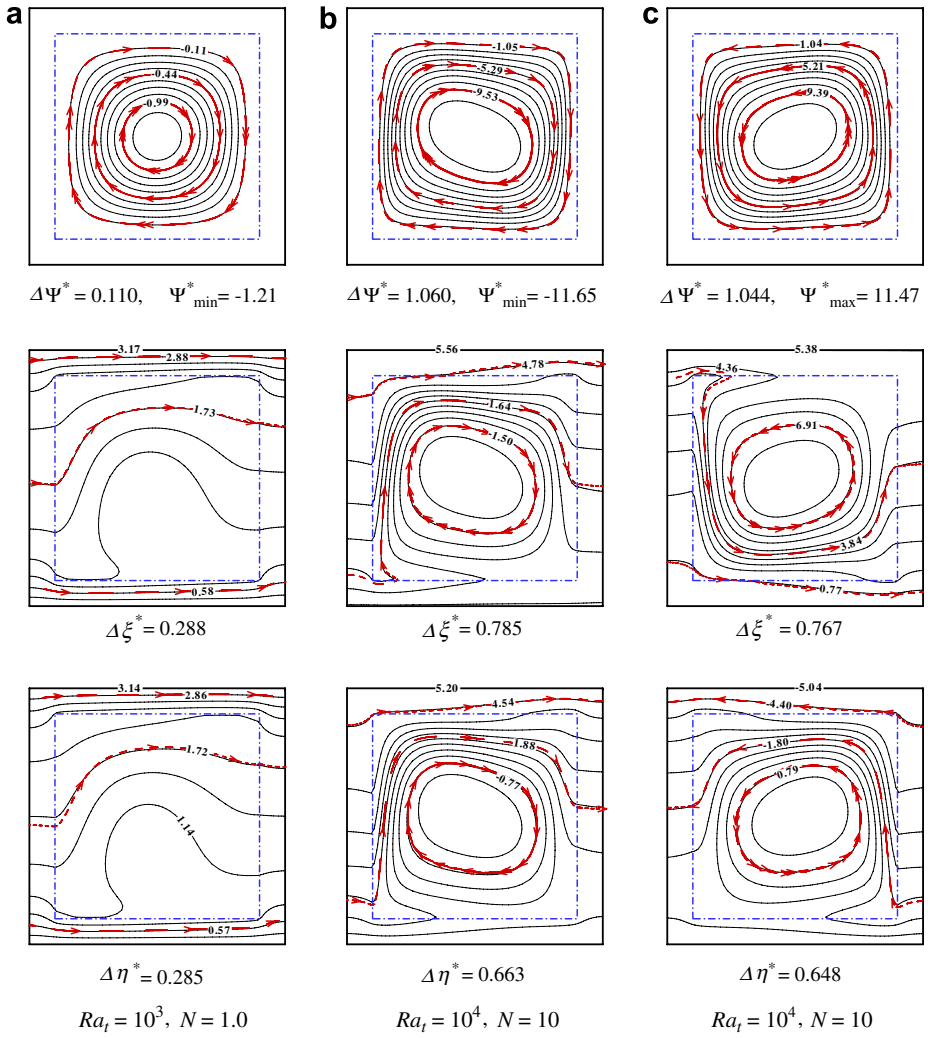


Fig. 5. Streamlines (top), heatlines (center) and masslines (bottom) for aiding (a and b) and opposing (c) buoyancy effects in Case B. $R_k$ and $R_D$ are both maintained at 10.0. Base legend as in Fig. 4.

closed counter-clockwise loop on the masslines is placed near the right vertical wall, of highest concentration level. Heat flows mainly through a thin region close to the lower horizontal wall, and mass flows mainly through a thin region close to the upper horizontal wall of the enclosure.

*6.2.2. Case B – square enclosure encircled with finite walls*

The inner square cavity filled with fluid mixture is centered in the enclosure. The void fraction, acreage ratio of inner cavity to the external enclosure, is fixed at 0.64. The thermal conductivity ratio ($R_k$) and solutal diffusion ratio ($R_D$) are both maintained at 10.0.

As presented in Fig. 5, visualization lines from Poisson equation method and integration method would coincide with each other. However, with the enhanced convection, there would exist differences, especially for heatlines and masslines presented in Fig. 5(b) and (c), which would attributes to the convergence errors resulted from higher Rayleigh number and buoyancy ratio. Comparing with pure double diffusive natural convection, conjugate heat and mass transfer problems can provoke the unique convergence issue for coupling of momentum and pressure. In other words, the convergence accuracy can be explicitly embodied by function contours calculated from different methods [32,36]. Essentially, the Poisson method, Eq. (7) of function $\Phi$ cannot be set up until the variable $\phi$ is continuous to its second-order derivatives all over the domain, while the integration method, Eq. (12), has no such inhibition.

At small $Ra_t$ ($10^3$) and low buoyancy ratio ($N = 1$), there are little heat and mass transfer between the top horizontal wall and the fluid, with sparse heatlines and masslines crossing that top interface shown in Fig. 5(a).

With the increased $Ra_t$ and $N$, as illustrated in Fig. 5(b), the heat and solutal flows by convective transportation cluster to the top horizontal wall, while the heat conduction and solutal diffusion are dominant in the center of cavity. This is due to the fact that as the fluid sweeps the left vertical wall it becomes heated and soluted, the boundary layer would become thinner with increasing $Ra_t$ and $N$.

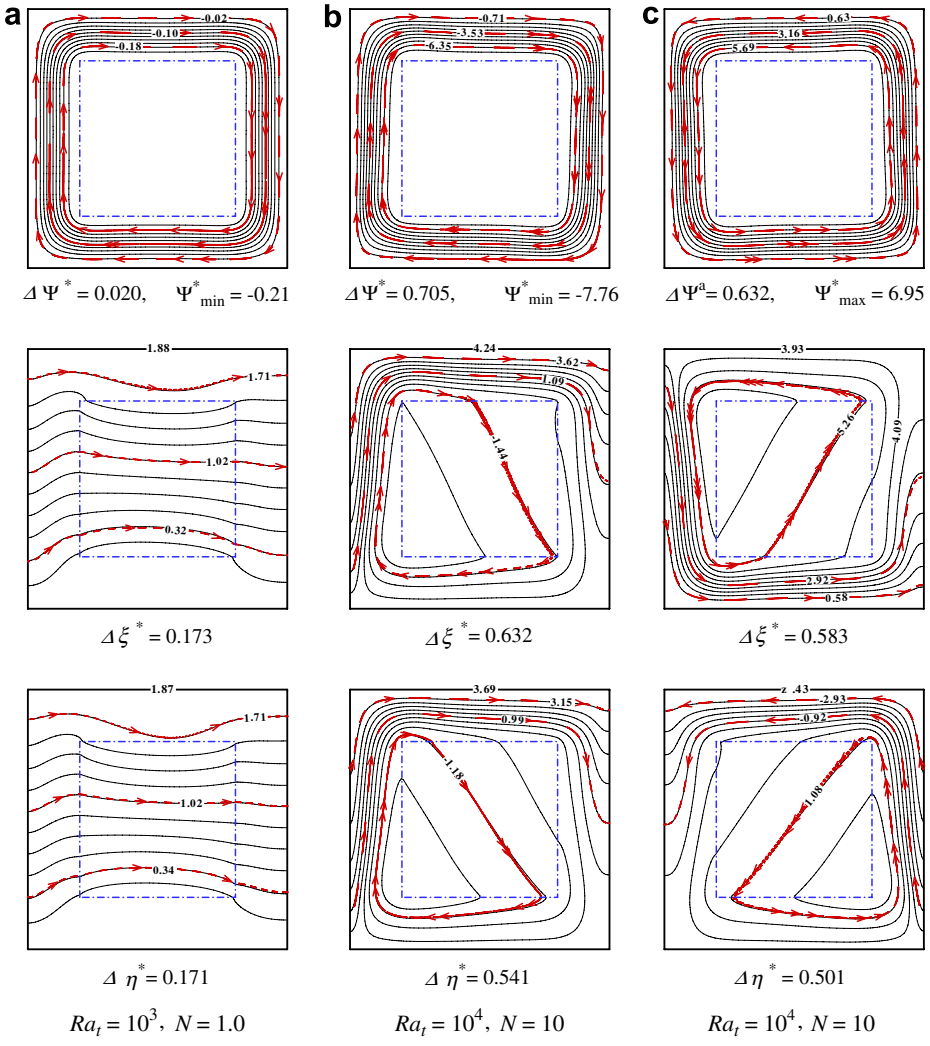


Fig. 6. Streamlines (top), heatlines (center) and masslines (bottom) for aiding (a and b) and opposing (c) buoyancy effects in Case C. $R_k$ and $R_D$ are both maintained at 10.0. Base legend as in Fig. 4.

As the fluid flows along the upper wall it continues to be heated and soluted until at some point it begins to release some of its energy and solute to the wall, where heatline and massline are penetrating from fluid to the wall. The fluid flowing down along the cold and lower-concentration vertical wall continues to release some of its energy and solute. As the cold and low-concentration fluid sweeps the bottom horizontal wall, the direction of heat and mass transfer should be from the wall to fluid, but it is still from the fluid to the wall after fluid travels near the left side. The heatlines and masslines show that there are little heat and mass exchanges between the fluid and the bottom horizontal wall.

Fig. 5(c) presents the situation corresponding to the opposite buoyancy effects, with a buoyancy ratio $N = 10$. The temperature and concentration contour plots (not shown) also take the form of the mirror images corresponding to these associated with the pure natural convection heat transfer problem for $Ra_t = 10^5$, as well as the global Nusselt number, 5.38 in present situation and 5.27 in pure thermal natural convection [24,37]. Drastic changes for heatlines and masslines also take place, similarly as reported for pure double diffusive natural convection in square enclosures.

#### 6.2.3. Case C – square enclosure with centered solid body

The fluid-saturated square enclosure is centered with one square conducting body. The solid occupied volume ratio, the thermal conductivity and solutal diffusion ratio are maintained at 0.36, 10.0 and 10.0 respectively.

When the Rayleigh number and combined buoyant ratio are low, $Ra_t = 10^3$ and $N = 1.0$, the existence of a conducting body reduces the convection, with the maximum value of absolute streamfunction $|\Psi|_{max}$ decreasing to 0.21 in Fig. 6(a), from 2.07 in Fig. 4(a). Thus, conduction and diffusion play a fully dominant role in the process of heat and mass transfer. For higher thermal and mass diffusion ratios of solid body, the total Nusselt number and Sherwood number increase to 1.88 and 1.87 from 1.33 and 1.23 respectively. Accordingly, the heatlines and masslines basically follow the principle of heat conduction and mass diffusion, largely exhibiting parallel lines.

As can be seen from the heatlines and masslines shown in Fig. 6(b), the solid body directly conducts heat and solute from the hot and higher-concentration fluid near the top-left wall to the cold and lower-concentration fluid adjacent bottom-right wall, which acts like "short circuiting". The thermal conduction and solutal diffusion of solid body reduce the temperature and concentration differences between the two sides, and eventually degrade the strength of convection as compared to the pure double diffusive convection at $Ra_t = 10^4$ and $N = 10$, with the maximum absolute streamfunction $|\Psi|_{max}$ decreasing from 11.40 to 7.76. The overall heat and mass transfer across the enclosure, represented by the overall Nusselt and Sherwood numbers, decreases to $Nu = 4.24$ and $Sh = 3.69$, 13% and 17% lower than that for pure double diffusive convection.

Fig. 6(c) presents the situation corresponding to the opposite buoyancy effects, with a buoyancy ratio $N = 10$. Drastic changes for heatlines and masslines also take place, similar as the aforementioned opposed buoyancy flows.

## 7. Concluding remarks

This study has presented some implementational issues and applications related to streamlines, heatlines and masslines.

The function diffusion coefficients are uniquely obtained from the diffusion coefficients of the corresponding primitive variables, $\Gamma_\Phi = 1/\Gamma_\phi$, harmonic mean practice of function coefficients at interfaces of solid and fluid regions is recommended. The function lines can be obtained by Poisson method and integration method. Streamlines would only be valid in fluid regions, while heatlines and masslines can penetrate the solid blocks. Appropriate dimensionless forms of heatfunction and massfunction would match the spatial Nusselt and Sherwood numbers, respectively.

Broader applications of double diffusive conjugate natural convection have validated the solution strategies. Convergence errors can be explicitly embodied by differences of function contours calculated by different methods. The overall Nusselt and Sherwood numbers can be read directly from the contours along the horizontal top wall. The streamlines, heatlines and masslines provide a more practical and efficient way to visualize the results than the customary ones. Visualization results by streamlines, heatlines and masslines directly exhibit the nature of fluid, and heat and mass transports through each cavity and also through the diffusive walls and solid bodies, and thus provides more vigorous means to discuss the convective heat and mass transfer.

## Acknowledgements

The authors wish to express their appreciation for support from the National Natural Science Foundation of China (No. 50578059). The authors are also grateful to the anonymous referees who provided detailed and constructive comments.

## References

[1] S. Kimura, A. Bejan, The "Heatline" visualization of convective heat transfer, J. Heat Transfer 105 (1983) 916–919.
[2] A. Bejan, Convection Heat Transfer, first ed., Wiley, New York, 1984.
[3] D.V. Trevisan, A. Bejan, Combined heat and mass transfer by natural convection in a vertical enclosure, J. Heat Transfer 109 (1987) 104–112.
[4] D. Littlefield, P. Desai, Buoyant laminar convection in a vertical cylindrical annulus, J. Heat Transfer 108 (1986) 814–821.
[5] F.L. Bello-Ochende, A heatfunction formulation for thermal convection in a square cavity, Comput. Methods Appl. Mech. Eng. 68 (1988) 141–149.
[6] S.K. Aggarwal, A. Manhapra, Use of heatlines for unsteady buoyancy-driven flow in a cylindrical enclosure, J. Heat Transfer 111 (1989) 576–578.

[7] S.K. Aggarwal, A. Manhapra, Transient natural convection in a cylindrical enclosure nonuniformly heated at the top wall, Numer. Heat Transfer, Part A 15 (1989) 341–356.
[8] C.J. Ho, Y.H. Lin, A numerical study of natural convection in concentric and eccentric horizontal cylindrical annuli with mixed boundary conditions, Int. J. Heat Fluid Flow 10 (1989) 40–47.
[9] C.J. Ho, Y.H. Lin, Natural convection of cold water in a vertical annulus with constant heat flux on the inner wall, J. Heat Transfer 112 (1990) 117–123.
[10] Al.M. Morega, A. Bejan, Heatline visualization of forced convection boundary layers, Int. J. Heat Mass Transfer 36 (1993) 3957–3966.
[11] Al. M. Morega, A. Bejan, Heatline visualization of forced convection in porous media, Int. J. Heat Fluid Flow 15 (1994) 42–47.
[12] V.A.F. Costa, Heatline and massline visualization of laminar natural convection boundary layers near a vertical wall, Int. J. Heat Mass Transfer 43 (2000) 3765–3774.
[13] S.K. Dash, Heatline visualization in turbulent flow, Int. J. Numer. Methods Heat Fluid Flow 6 (1996) 37–46.
[14] A. Bejan, Convection Heat Transfer, second ed., Wiley, New York, 1995.
[15] V.A.F. Costa, Unification of the streamline, heatline and massline methods for the visualization of two-dimensional transport phenomena, Int. J. Heat Mass Transfer 42 (1999) 27–33.
[16] S.J. Kim, S.P. Jang, Experimental and numerical analysis of heat transfer phenomena in a sensor tube of a mass flow controller, Int. J. Heat Mass Transfer 44 (2001) 1711–1724.
[17] Q.H. Deng, G.F. Tang, Numerical visualization of mass and heat transport for conjugate natural convection/heat conduction by streamline and heatline, Int. J. Heat Mass Transfer 45 (2002) 2373–2385.
[18] V.A.F. Costa, Comment on paper Qi-Hong Deng, Guang-Fa Tang, Numerical visualization of mass and heat transport for conjugate natural convection/heat conduction by streamline and heatline, Int. J. Heat Mass Transfer 46 (2003) 185–187.
[19] V.A.F. Costa, Unified streamline, heatline and massline methods for the visualization of two-dimensional heat and mass transfer in anisotropic media, Int. J. Heat Mass Transfer 46 (2003) 1309–1320.
[20] A. Mukhopadhyay, X. Qin, S.K. Aggarwal, I.K. Puri, On extension of "heatline" and "massline" concepts to reacting flows through use of conserved scalars, J. Heat Transfer 124 (2002) 791–799.
[21] A. Mukhopadhyay, X. Qin, I.K. Puri, S.K. Aggarwal, Visualization of scalar transport in non-reacting and reacting jets through a unified "heatline" and "massline" formulation, Numer. Heat Transfer, Part A 44 (2003) 683–704.
[22] H. Chattopadhyay, S.K. Dash, Numerical visualization of convective heat transfer from a sphere – with and without radial mass flux, Int. J. Numer. Methods Heat Fluid Flow 5 (1995) 705–716.
[23] H.Y. Wang, F. Penot, J.B. Sauliner, Numerical study of a buoyancy-induced flow along a vertical plate with discretely heated integrated circuit packages, Int. J. Heat Mass Transfer 40 (1997) 1509–1520.
[24] V.A.F. Costa, Double diffusive natural convection in a square enclosure with heat and mass diffusive walls, Int. J. Heat Mass Transfer 40 (1997) 4061–4071.
[25] V.A.F. Costa, Double diffusive natural convection in parallelogrammic enclosure, Int. J. Heat Mass Transfer 47 (2004) 2913–2926.
[26] V.A.F. Costa, M.S.A. Oliveira, A.C.M. Sousa, Laminar natural convection in a vertical stack of parallelogrammic partial enclosures with variable geometry, Int. J. Heat Mass Transfer 48 (2005) 779–792.
[27] S.V. Patankar, Numerical Heat Transfer and Fluid Flow, Hemisphere, Washington, DC, 1980.
[28] F.Y. Zhao, L. Zhang, G.F. Tang, J.L. Lu, Numerical simulation of airflow in partitioned enclosures at high Rayleigh numbers, in: Proc. Energy and Environment 2003, Science Press, New York, 2003, pp. 139–143.
[29] F.Y. Zhao, G.F. Tang, D. Liu, Mixed convection and conjugate heat transfer in multi air ducts of thermoelectric refrigerator, HV&AC 35 (2005) 12–17.
[30] W.Q. Tao, Numerical Heat Transfer, second ed., Xi'an Jiaotong University Press, Xi'an, 2002.
[31] F.Y. Zhao, G.F. Tang, D. Liu, Conjugate natural convection in enclosures with external and internal heat sources, Int. J. Eng. Sci. 44 (2006) 148–165.
[32] F.Y. Zhao, Numerical Simulation of Thermal Environment in Urban Residential District. M.S. Thesis, Hunan University, PR China, 2003.
[33] S. Thakur, W. Shyy, Some implementational issues of convection schemes for finite-volume formulations, Numer. Heat Transfer, Part B 24 (1993) 31–55.
[34] M. Benzeghiba, S. Chikh, A. Campo, Thermosolutal convection in a partly porous vertical annular cavity, J. Heat Transfer 125 (2003) 703–715.
[35] C. Beghein, F. Haghighat, F. Allard, Numerical study of double diffusive natural convection in a square cavity, Int. J. Heat Mass Transfer 35 (1992) 833–846.
[36] F.Y. Zhao, D. Liu, G.F. Tang, Conjugate heat transfer in square enclosures, Heat Mass Transfer, in press, doi:10.1007/s00231-006-0136-4.
[37] D.M. Kim, R. Viskanta, Study of the effects of wall conductance on natural convection in differently oriented square cavities, J. Fluid Mech. 144 (1984) 153–176.